

Simplicity Prevails: The Emergence of Generalizable AIGI Detection in Visual Foundation Models

Yue Zhou¹ Xinan He² ¹ Kaiqing Lin¹ Bing Fan³ Feng Ding² Bin Li¹

Abstract

While specialized detectors for AI-Generated Images (AIGI) achieve near-perfect accuracy on curated benchmarks, they suffer from a dramatic performance collapse in realistic, in-the-wild scenarios. In this work, we demonstrate that simplicity prevails over complex architectural designs. A simple linear classifier trained on the frozen features of modern Vision Foundation Models , including Perception Encoder, MetaCLIP 2, and DINOv3, establishes a new state-of-the-art. Through a comprehensive evaluation spanning traditional benchmarks, unseen generators, and challenging in-the-wild distributions, we show that this baseline not only matches specialized detectors on standard benchmarks but also decisively outperforms them on in-the-wild datasets, boosting accuracy by striking margins of over 30%. We posit that this superior capability is an emergent property driven by the massive scale of pre-training data containing synthetic content. We trace the source of this capability to two distinct manifestations of data exposure: Vision-Language Models internalize an explicit semantic concept of forgery, while Self-Supervised Learning models implicitly acquire discriminative forensic features from the pretraining data. However, we also reveal persistent limitations: these models suffer from performance degradation under recapture and transmission, remain blind to VAE reconstruction and localized editing. We conclude by advocating for a paradigm shift in AI forensics, moving from overfitting on static benchmarks to harnessing the evolving world knowledge of foundation models for real-world reliability.

¹Guangdong Provincial Key Laboratory of Intelligent Information Processing, Shenzhen Key Laboratory of Media Security, and SZU AFS Joint Innovation Center for AI Technology, Shenzhen University ²Nanchang University ³University of North Texas. Correspondence to: Bin Li <libin@szu.edu.cn>, Feng Ding <fengding@ncu.edu.cn>.

Preprint. February 3, 2026.

1. Introduction

“One thing that should be learned from the bitter lesson is the great power of general purpose methods, of methods that continue to scale with increased computation even as the available computation becomes very great.”

— Rich Sutton, *The Bitter Lesson* (Sutton, 2019)

The rapid evolution of generative models, such as Midjourney, Stable Diffusion (Rombach et al., 2021) and Nano Banana(Team et al., 2023), has ushered in a new era of content creation, synthesizing photorealistic images that challenge the boundaries of visual authenticity. While empowering creativity, this technological leap simultaneously introduces profound threats to information integrity, fueling the proliferation of misinformation and deepfakes. In response, the forensics community has largely favored a specialized approach: crafting detectors with increasingly complex module tailored to specific artifacts, such as frequency anomalies or noise residuals (Wang et al., 2020; Ju et al., 2022). While these specialized detectors achieve near-perfect accuracy on curated benchmarks, they often suffer from a dramatic performance collapse in realistic scenarios. Recent studies, such as the Chameleon benchmark (Yan et al., 2024a), reveal that detectors excelling in controlled environments frequently degrade to 60%–70% accuracy when deployed ‘in-the-wild’. This fragility suggests that relying on hand-crafted inductive biases may be a dead end in the face of rapidly evolving generative distributions.

Echoing Sutton’s “Bitter Lesson”, we present a finding that challenges this trend: **simplicity prevails**. We demonstrate that a simple linear classifier, trained on top of frozen features from **modern Vision Foundation Models (VFM**s), achieves state-of-the-art performance. We define modern VFM as the latest generation of encoders, such as Perception Encoder (PE) (Bolya et al., 2025), MetaCLIP 2 (Chuang et al., 2025), and DINOv3 (Siméoni et al., 2025), which have been exposed to billion-scale web data. Our evaluation spans three distinct protocols: standard benchmarks (e.g., GenImage (Zhu et al., 2023)), datasets from the latest unseen generators (e.g., AIGIHolmes (Zhou et al., 2025b), AIGI-Now (Chen et al., 2025a)), and challenging in-the-wild distributions (e.g., Chameleon(Yan et al., 2024a),

WildRF(Cavia et al., 2024)). Across all settings, this simple baseline matches or decisively outperforms specialized detectors, boosting accuracy by margins of over 30% in the most difficult in-the-wild scenarios.

We posit that this superior capability is not an architectural innovation for forensics but an **emergent property** derived from the massive scale of pre-training data. Through rigorous analysis of the Common Crawl index¹, we observe an exponential explosion of generative content in web corpora starting from 2022. Modern VFM, trained on this evolving data landscape, have inadvertently internalized the necessary concepts to distinguish synthetic content. We trace the source of this capability to two distinct manifestations of data exposure. For Vision-Language Models, the co-occurrence of synthetic images and textual descriptions leads to **explicit concept injection**, where the model aligns synthetic visuals with high-level forgery concepts. For Self-Supervised Learning (SSL) models like DINOv3, the capability emerges from **implicit distribution fitting**, where the model encodes the distinct low-level signatures of the generative manifold in pretraining data.

Despite these significant gains, our analysis delineates the boundaries of this paradigm. We find that modern VFM remain **blind to pure reconstruction artifacts** and struggle with **localized editing**, while also suffering from performance degradation under aggressive real-world transmission and screen recapture. This suggests that while data scale has effectively solved the *generalizability* problem for fully synthetic content, the *localization* of fine-grained manipulation remains an open challenge. Therefore, we advocate for a paradigm shift in AI forensics: moving away from designing specialized architectures to chase benchmark metrics—since simple backbones already suffice for global detection—and instead focusing on how to harness and refine the evolving world knowledge of foundation models to address these fine-grained forensic tasks.

In summary, our main contributions are:

- We establish the superiority of simple linear probes on modern VFM over specialized detectors. Across a comprehensive evaluation spanning standard benchmarks, previously unseen generators, and challenging in-the-wild distributions, our baseline achieves SOTA performance, outperforming specialized methods by margins of over 30% in realistic scenarios.
- We trace the source of this capability to pre-training data exposure rather than architectural design. We identify two emergent mechanisms: **explicit concept injection** in Vision Language Models and **implicit distribution fitting** in Self-Supervised Learning Models.

- We delineate the **boundaries of this paradigm**, revealing persistent blind spots in pure reconstruction and localized editing. We conclude that future research should shift focus from designing complex architectures to harnessing the evolving world knowledge of foundation models for fine-grained forensic tasks.

2. Related Works

The development of AI-generated image (AIGI) detection has undergone a significant paradigm shift, evolving from hand-crafted artifact analysis to the adaptation of large-scale foundation models.

Early Artifact-Based Detection. Initial forensic methods focused on identifying the low-level imperfections inherent to early generative architectures. Researchers found that up-sampling operations in GANs and CNNs often leave distinct footprints, such as checkerboard artifacts in the pixel space (Odena et al., 2016) or spectral anomalies in the frequency domain (Frank et al., 2020). Others exploited inconsistencies in color statistics (McCloskey & Albright, 2019) or noise residuals (Cozzolino & Verdoliva, 2019) to distinguish synthetic content. While effective against specific generators, these hand-crafted features proved brittle against the rapid evolution of generative models, particularly with the advent of Diffusion Models which exhibit fundamentally different artifact patterns.

Data-Driven Specialized Detectors. With the dominance of Diffusion Models, the focus shifted from detecting CNN-specific upsampling artifacts (e.g., checkerboard patterns in GANs (Wang et al., 2020)) to identifying the unique traces of the diffusion process. Researchers proposed reconstructing input images to isolate generative errors: DIRE (Wang et al., 2023) leverages the reconstruction residual from a pre-trained diffusion model as a forensic signal, while DRCT (Chen et al., 2024a) refines this by analyzing the discrepancies between real-real and fake-fake reconstruction pairs. Others focused on improving generalization: SAFE (Li et al., 2025b) introduces artifact-preserving augmentations to decouple semantic content from forensic traces. notably, DDA (Chen et al., 2025b) targets the shared VAE decoder inherent to Latent Diffusion Models, explicitly aligning the detector with VAE reconstruction patterns to achieve broader generalization across different LDM-based generators.

The Foundation Model Era. The introduction of Uni-vFD (Ojha et al., 2023) marked a pivotal turning point. Ojha et al. revealed that training a linear layer on top of the frozen feature space of a pre-trained Vision-Language Model (specifically CLIP (Radford et al., 2021)) yields significantly better generalization than training CNNs from scratch. This discovery spurred a wave of research leverag-

¹Common Crawl Index Server <https://index.commoncrawl.org/>

Table 1. Performance on GenImage Benchmark. All detectors are trained on Stable Diffusion v1.4 and evaluated on unseen generators. Accuracy is averaged over real and fake classes. Best results in **bold**.

Method	ADM	BigGAN	Midjourney	VQDM	GLIDE	SD-v1.4	SD-v1.5	Wukong	Avg.
<i>Modern VFM Baselines (Ours)</i>									
MetaCLIP-Linear	0.549	0.524	0.839	0.653	0.653	0.984	0.981	0.942	0.766
MetaCLIP2-Linear	0.690	0.816	0.959	0.819	0.887	0.993	0.991	0.980	0.892
SigLIP-Linear	0.740	0.658	0.812	0.857	0.916	0.955	0.954	0.918	0.851
SigLIP2-Linear	0.870	0.924	0.879	0.954	0.951	0.995	0.995	0.994	0.945
PE-CLIP-Linear	0.712	0.963	0.901	0.959	0.972	0.999	0.999	0.999	0.938
DINOv2-Linear	0.651	0.889	0.811	0.757	0.852	0.967	0.961	0.929	0.852
DINOv3-Linear	0.849	0.991	0.934	0.992	0.963	0.998	0.996	0.994	0.964
<i>Competitor Methods</i>									
CNNSpot (Wang et al., 2020)	0.507	0.530	0.610	0.501	0.522	0.998	0.996	0.985	0.706
FreqNet (Tan et al., 2024a)	0.608	0.939	0.849	0.626	0.858	0.950	0.949	0.937	0.840
Gram-Net (Liu et al., 2020)	0.576	0.591	0.665	0.528	0.747	0.989	0.988	0.960	0.756
NPR (Tan et al., 2024b)	0.619	0.849	0.850	0.567	0.844	0.996	0.994	0.984	0.838
UnivFD (Ojha et al., 2023)	0.571	0.839	0.795	0.644	0.842	0.959	0.958	0.926	0.817
SAFE (Li et al., 2025b)	0.600	0.880	0.829	0.708	0.836	0.964	0.967	0.903	0.836
LaDeDa (Cavia et al., 2024)	0.512	0.583	0.595	0.513	0.585	0.876	0.871	0.820	0.670
Effort (Yan et al., 2024b)	0.704	0.749	0.756	0.824	0.807	0.874	0.873	0.867	0.807
DDA (Chen et al., 2025b)	0.880	0.741	0.960	0.719	0.862	0.986	0.985	0.986	0.890
OMAT (Zhou et al., 2025a)	0.837	0.973	0.903	0.954	0.974	0.974	0.973	0.975	0.946
AIDE (Yan et al., 2024a)	0.602	0.648	0.813	0.694	0.514	0.959	0.957	0.954	0.768

ing Vision Foundation Models (VFs) as backbones. Subsequent works, such as Effort (Yan et al., 2024b), AIDE (Yan et al., 2024a), OMAT (Zhou et al., 2025a) and DDA (Chen et al., 2025b), have explored various strategies to adapt CLIP or DINOv2 (Oquab et al., 2023) for forensics, including prompt tuning, adapter modules, fusing frequency-domain information and training hard samples. These methods currently represent the state-of-the-art, yet as our experiments show, they still struggle to maintain robustness in unconstrained, in-the-wild scenarios compared to the raw capabilities of the latest VFs. (See Appendix A for a comprehensive survey of the legacy backbones still prevalent in these recent methods.)

3. Simplicity Prevails: Benchmarking Modern VFs

To empirically validate our hypothesis that the generalization capability of AIGI detection stems from the scale of pre-training data rather than complex architectural designs, we conduct a comprehensive comparative analysis. We pit simple linear classifiers trained on modern Vision Foundation Models (VFs) against a wide array of state-of-the-art specialized detectors. Our evaluation protocol is designed to be rigorous and progressively challenging, spanning three distinct scenarios: standard academic benchmarks, realistic in-the-wild distributions, and unseen next-generation generative models. In this section, we detail our experimental setup and present the performance comparisons that establish the superiority of modern VF baselines.

3.1. Experimental Setup

Evaluation Benchmarks. To rigorously assess generalization, we organize our evaluation into three progressively

challenging categories. (1) **Standard Benchmarks:** We use **GenImage** (Zhu et al., 2023), a widely adopted benchmark comprising images from 8 generators (e.g., Stable Diffusion, Midjourney). Following standard protocols (Ojha et al., 2023), we use the Stable Diffusion v1.4 subset for training and the remaining subsets for testing. (2) **In-the-Wild Datasets:** We evaluate on **Chameleon** (Yan et al., 2024a), **WildRF** (Cavia et al., 2024), SocialRF and **CommunityAI** (Li et al., 2025d). These datasets are collected from social media and internet forums, featuring diverse, unconstrained post-processing and unknown generative sources, representing a realistic detection scenario. (3) **Unseen Generators:** We employ **AIGIHolmes** (Zhou et al., 2025b) and **AIGI-Now** (Chen et al., 2025a), recent benchmarks containing images from state-of-the-art generators released after 2024, including close source generators like Nano Banana, GPT4o and FLUX-Pro. These serve as a strict test for generalization to unseen distributions.

Specialized Detectors. We compare against a comprehensive suite of state-of-the-art forensic methods, spanning three categories: (1) **Specialized Detectors:** Artifact-based methods like CNNSpot (Wang et al., 2020), FreqNet (Tan et al., 2024a), and NPR (Tan et al., 2024b), as well as recent VF-based adapters such as UnivFD (Ojha et al., 2023), OMAT (Zhou et al., 2025a), Effort (Yan et al., 2024b) and Dual-Data-Alignment (DDA) (Chen et al., 2025b). (2) **Former VF Baselines:** To explicitly evaluate the impact of pre-training data evolution, we include earlier generations of foundation models, such as the original OpenAI CLIP (Radford et al., 2021), SigLIP (Zhai et al., 2023), Meta CLIP (Xu et al., 2023a) and DINOv2 (Oquab et al., 2023). For DDA, we utilize the official pre-trained weights provided by the authors, as its core contribution involves a specialized training pipeline with VAE-reconstructed data alignment. All other

Table 2. Performance on In-the-Wild Benchmarks. Evaluation on Chameleon, WildRF, SocialRF, and CommunityAI datasets. Accuracy is averaged over real and fake classes. Best results in **bold**.

Method	Chameleon			WildRF			SocialRF			CommunityAI			Avg.
	Real	Fake	Avg.										
<i>Modern VFM Baselines (Ours)</i>													
MetaCLIP-Linear	0.373	0.914	0.644	0.461	0.923	0.692	0.409	0.866	0.638	0.353	0.933	0.643	0.654
MetaCLIP2-Linear	0.948	0.913	0.930	0.478	0.979	0.728	0.659	0.940	0.800	0.926	0.954	0.940	0.842
SigLIP-Linear	0.480	0.732	0.606	0.383	0.897	0.640	0.549	0.613	0.581	0.370	0.857	0.614	0.610
SigLIP2-Linear	0.884	0.833	0.859	0.597	0.984	0.790	0.744	0.866	0.805	0.826	0.905	0.866	0.822
PE-CLIP-Linear	0.970	0.948	0.959	0.679	0.994	0.836	0.751	0.970	0.861	0.966	0.975	0.971	0.899
DINOv2-Linear	0.628	0.580	0.608	0.643	0.772	0.705	0.603	0.695	0.649	0.606	0.562	0.583	0.636
DINOv3-Linear	0.933	0.895	0.914	0.948	0.975	0.961	0.937	0.948	0.943	0.949	0.946	0.948	0.940
<i>Competitor Methods</i>													
CNNSpot	0.979	0.128	0.554	0.959	0.290	0.625	0.588	0.541	0.565	0.969	0.112	0.541	0.571
FreqNet	0.985	0.090	0.538	0.731	0.559	0.645	0.544	0.553	0.549	0.977	0.128	0.553	0.571
Gram-Net	0.992	0.044	0.518	0.947	0.205	0.576	0.531	0.523	0.527	0.985	0.061	0.523	0.536
NPR	0.999	0.046	0.523	0.980	0.243	0.612	0.593	0.537	0.565	0.998	0.076	0.537	0.560
UnivFD	0.763	0.441	0.602	0.693	0.637	0.665	0.563	0.637	0.600	0.778	0.495	0.636	0.617
SAFE	0.993	0.046	0.520	0.918	0.309	0.613	0.564	0.532	0.548	0.984	0.080	0.532	0.556
LaDeDa	0.994	0.015	0.504	0.988	0.119	0.554	0.542	0.506	0.524	0.986	0.026	0.506	0.523
Effort	0.394	0.782	0.588	0.179	0.955	0.567	0.513	0.533	0.523	0.225	0.840	0.533	0.553
DDA	0.940	0.708	0.824	0.899	0.908	0.904	0.818	0.846	0.832	0.968	0.725	0.847	0.850
OMAT	0.899	0.359	0.629	0.633	0.715	0.674	0.581	0.633	0.607	0.853	0.414	0.634	0.636
AIDE	0.944	0.203	0.574	0.973	0.195	0.584	0.578	0.541	0.560	0.990	0.093	0.542	0.565

methods are trained on GenImage stable_diffusion_v_1.4 training set for fair comparison.

Modern VFM Baselines. To test our “Simplicity Prevails” hypothesis, we select a representative set of modern Vision Foundation Models as frozen feature extractors. These include **Vision-Language Models** (CLIP (Radford et al., 2021), SigLIP2 (Tschannen et al., 2025), MetaCLIP 2 (Chuang et al., 2025), Perception Encoder (Boyle et al., 2025)) and **Self-Supervised Models** (DINOv2 (Oquab et al., 2023), DINOv3 (Siméoni et al., 2025)). We attach a simple linear layer to the pooled output features of these backbones. Detailed specifications of model architectures and pre-training datasets are provided in Appendix C.

Implementation Details. All our VFM baselines are trained solely on the **GenImage (SD v1.4)** training set. We keep the backbone completely frozen and only update the linear head. We use the AdamW optimizer with a learning rate of $1e^{-3}$ and a batch size of 128 for 2 epoch. Images are resized and center-cropped to the native resolution of each model without any additional data augmentation.

3.2. Performance on Standard Benchmarks

We first establish the efficacy of our simple baselines on the standard GenImage benchmark in Table 1. Despite the simplicity of the linear probe, modern VFM baselines achieve state-of-the-art performance. DINOv3-Linear reaches the highest average accuracy of 96.5%, surpassing the best specialized detector OMAT (94.6%) and significantly outperforming legacy baselines. Notably, we observe a substantial performance leap across VFM generations: DINOv3 improves upon DINOv2 by over 11%, and MetaCLIP-2 boosts accuracy by 12.6% compared to its predecessor MetaCLIP. This

trend highlights that forensic discriminability is not static but scales with the quality and data volume of the foundation model. Furthermore, while specialized detectors often overfit to the training source, modern VFM baselines demonstrate robust generalization across diverse generative architectures, confirming that their representations are inherently forensic-ready without the need for complex auxiliary modules.

3.3. The Collapse of SOTA in the Wild

While standard benchmarks provide a controlled environment, real-world deployment involves diverse, unconstrained data distributions. To evaluate this, we test on four challenging in-the-wild datasets: **Chameleon**, **WildRF**, **Social-RF**, and **CommunityAI**. The results, summarized in Table 2, reveal a stark contrast. **Results.** Most specialized detectors suffer a catastrophic performance collapse. Methods like NPR, LaDeDa, and even recent techniques like OMAT degrade to near-random performance, primarily due to a failure to recognize diverse fake samples. The only exception among specialized methods is DDA, which maintains a respectable average accuracy of 85.0%, due to its alignment with the robust VAE decoder patterns shared across latent diffusion models by training on DINOv2 with VAE reconstruct data.

However, modern VFM baselines decisively outperform all competitors. DINOv3-Linear achieves an average accuracy of 94.0%, surpassing DDA by nearly 10% and traditional detectors by over 30%. Crucially, we observe a massive performance gap between modern and legacy VFM baselines: DINOv3 outperforms its predecessor DINOv2 by a staggering 30.4%, and MetaCLIP-2 surpasses MetaCLIP by 18.8%. This confirms that earlier foundation models lacked the necessary data exposure to handle in-the-wild shifts, whereas mod-

Table 3. Generalization on AIGIHolmes. Evaluation on advanced auto-regressive and diffusion-transformer generative models. Accuracy is averaged over real and fake classes. Best results in **bold**.

Detector	FLUX	Infinity	Janus	Janus-Pro-1B	Janus-Pro-7B	LlamaGen	PixArt-XL	SD3.5-L	Show-o	VAR	Avg
<i>Modern VFM Baselines (Ours)</i>											
MetaCLIP-Linear	0.951	0.978	0.736	0.950	0.950	0.970	0.970	0.867	0.972	0.614	0.896
MetaCLIP2-Linear	0.987	0.990	0.839	0.959	0.928	0.989	0.986	0.956	0.985	0.802	0.942
SigLIP-Linear	0.888	0.918	0.889	0.928	0.926	0.913	0.896	0.826	0.868	0.834	0.889
SigLIP2-Linear	0.957	0.994	0.990	0.993	0.989	0.991	0.994	0.914	0.992	0.913	0.973
PE-CLIP-Linear	0.968	0.999	0.945	0.995	0.996	1.000	1.000	0.943	0.999	0.935	0.978
DINOv3-Linear	0.933	0.998	0.996	0.995	0.986	0.999	0.999	0.891	0.997	0.922	0.972
<i>Competitor Methods</i>											
CNNSpot	0.626	0.589	0.508	0.531	0.522	0.604	0.668	0.568	0.608	0.504	0.573
FreqNet	0.894	0.924	0.443	0.439	0.433	0.875	0.885	0.894	0.910	0.688	0.738
Gram-Net	0.696	0.604	0.491	0.491	0.491	0.627	0.627	0.701	0.771	0.557	0.606
NPR	0.968	0.983	0.495	0.495	0.495	0.947	0.899	0.937	0.988	0.730	0.794
LaDeDa	0.682	0.664	0.498	0.497	0.497	0.810	0.641	0.695	0.755	0.724	0.646
UnivFD	0.868	0.898	0.575	0.674	0.575	0.915	0.925	0.898	0.911	0.597	0.784
SAFE	0.932	0.965	0.482	0.482	0.483	0.913	0.896	0.940	0.962	0.911	0.796
Effort-AIGI	0.794	0.804	0.483	0.650	0.569	0.798	0.804	0.765	0.793	0.764	0.722
DDA	0.972	0.989	0.985	0.993	0.987	0.993	0.994	0.970	0.948	0.804	0.963
OMAT	0.947	0.955	0.651	0.756	0.641	0.967	0.969	0.957	0.969	0.959	0.877
AIDE	0.944	0.987	0.912	0.989	0.978	0.994	0.986	0.994	0.980	0.936	0.970

Table 4. Generalization on AIGI-Now. Evaluation on 9 open-source and close-source generative models. Accuracy is averaged over real and fake classes. Best results in **bold**.

Detector	FLUX-dev pix sem	FLUX-kera pix sem	FLUX-kontext pix sem	FLUX-pro pix sem	gpt4o pix sem	jimeng pix sem	keling pix sem	minimax pix sem	Nano pix sem	Avg
<i>Modern VFM Baselines (Ours)</i>										
MetaCLIP-Linear	0.948	0.965	0.956	0.913	0.708	0.808	0.894	0.943	0.898	0.882
MetaCLIP2-Linear	0.979	0.941	0.963	0.896	0.799	0.811	0.976	0.892	0.943	0.888
SigLIP-Linear	0.838	0.898	0.840	0.891	0.700	0.811	0.836	0.911	0.827	0.897
SigLIP2-Linear	0.947	0.882	0.883	0.697	0.776	0.678	0.888	0.885	0.936	0.790
PE-CLIP-Linear	0.977	0.959	0.918	0.762	0.830	0.774	0.873	0.943	0.863	0.924
DINOv3-Linear	0.944	0.962	0.846	0.811	0.730	0.756	0.813	0.948	0.898	0.960
<i>Competitor Methods</i>										
CNNSpot	0.919	0.500	0.550	0.500	0.843	0.502	0.535	0.500	0.990	0.501
FreqNet	0.875	0.468	0.697	0.443	0.769	0.479	0.492	0.501	0.923	0.510
Gram-Net	0.933	0.528	0.667	0.522	0.864	0.555	0.608	0.569	0.763	0.508
NPR	0.944	0.500	0.508	0.500	0.785	0.502	0.502	0.502	0.966	0.500
LaDeDa	0.586	0.498	0.497	0.497	0.560	0.502	0.496	0.495	0.745	0.499
UnivFD	0.542	0.579	0.514	0.538	0.492	0.545	0.516	0.544	0.529	0.532
SAFE	0.903	0.490	0.532	0.492	0.831	0.494	0.521	0.486	0.977	0.488
Effort-AIGI	0.789	0.679	0.796	0.669	0.728	0.610	0.688	0.690	0.753	0.580
DDA	0.916	0.512	0.594	0.499	0.827	0.529	0.766	0.550	0.923	0.654
OMAT	0.911	0.475	0.649	0.469	0.847	0.507	0.591	0.515	0.744	0.452
AIDE	0.991	0.590	0.504	0.569	0.979	0.806	0.601	0.538	0.747	0.518

ern iterations have internalized these distributions during pre-training.

3.4. Generalization to State-of-the-Art Generators

A critical question remains: do these models truly learn generalized forensic concepts, or do they merely memorize patterns seen during pre-training? To investigate this, we conduct a rigorous evaluation on **AIGIHolmes** and **AIGI-Now**. Crucially, these datasets contain:

- **Novel Architectures (AIGIHolmes):** Including recent Auto-Regressive (AR) models (e.g., **LlamaGen**, **VAR**) and Diffusion Transformers (e.g., **FLUX**, **PixArt-XL**), whose generation mechanisms differ fundamentally from the UNet-based diffusion models (e.g., **SD-v1.4**) dominant in older web corpora and common training data.

- **Proprietary Engines (AIGI-Now):** Including closed-source commercial APIs (e.g., **GPT-4o**, **Nano Banana**, **FLUX-Pro**), ensuring that their specific training data and artifacts were strictly inaccessible during the pre-training of our VFM backbones.

Results. As summarized in Tables 3 and 4, modern VFMs demonstrate exceptional transferability across these unseen domains. On AIGIHolmes, PE-CLIP-Linear and DINOv3-Linear achieve remarkable average accuracies of **97.8%** and **97.2%**. Notably, they maintain high performance even on Auto-Regressive models (e.g., **VAR**: 93.5%/92.2%), confirming that their learned features capture fundamental anomalies of synthesis rather than specific architecture-dependent artifacts. Similarly, on AIGI-Now, MetaCLIP2-Linear leads with **90.7%**, successfully detecting closed-source generators like GPT-4o. Conversely, specialized detectors struggle significantly, with methods like CNNSpot collapsing to near-random guessing (~57%) on

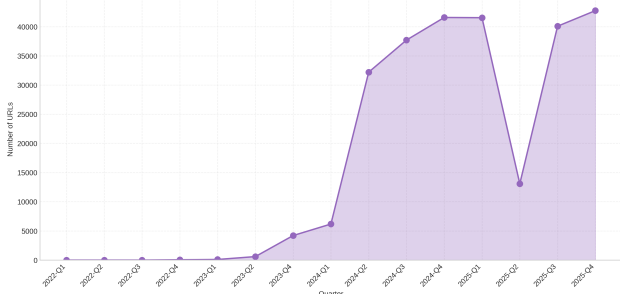


Figure 1. The Surge of Generative Data in Web Corpora. We track the number of indexed pages from `civitai.com` within Common Crawl snapshots from 2022 to 2025.

these novel distributions. This confirms that modern VFM_s have emerged with a generalized notion of artificiality that extends well beyond the specific generators seen during pre-training.

4. Analysis: The Mechanisms of Emergence

Our empirical results establish a counter-intuitive finding: simple linear probes on frozen Vision Foundation Models (VFM_s) consistently outperform specialized detectors that employ complex, domain-specific architectures. This raises a fundamental question regarding the nature of this capability. Is this an architectural superiority inherent to modern Transformers, or is it an artifact of the training data? In this section, we deconstruct the source of this generalizability and propose that the observed performance is not forensic “intelligence” in the traditional sense, but rather a direct manifestation of massive-scale data exposure.

4.1. The Source: An Explosion of Generative Content

To investigate synthetic data exposure in pre-training corpora, we analyzed the Common Crawl (CC) index, the primary data reservoir for models like MetaCLIP and DINOv3. Given the difficulty of quantifying in-the-wild AIGI, we use the indexing volume of `civitai.com`, the largest open-source generative model platform, as a proxy for the prevalence of high-quality synthetic content.

Figure 1 reveals a distinct phase shift. The pre-2022 “Silent Era” contained negligible generative content, explaining why legacy models like OpenAI CLIP lack forensic capability. In contrast, the period from 2023 to 2025 shows an exponential surge. Despite a transient dip in mid-2025 due to anti-crawling updates, the trajectory remains aggressively upward, peaking at over **40,000** indexed records per snapshot in late 2025. This rise directly correlates with the proliferation of tools like SDXL and FLUX.

This implies that modern VFM_s have been implicitly supervised on millions of AIGI samples alongside their textual

descriptions. This “contamination” effectively transforms unsupervised pre-training into a weakly-supervised detection task. We next trace how this exposure manifests in Vision-Language versus Self-Supervised Models.

4.2. Mechanism I: Semantic Conceptualization in VLMs

For Vision-Language Models (VLMs), we hypothesize that their capability stems from the contrastive pre-training objective. During training, massive volumes of synthetic images co-occur with metadata or captions containing explicit indicators of their source (e.g., *midjourney*, *AI generated*). Consequently, the model internalizes a powerful semantic shortcut: it learns to align the visual features of synthetic content directly with forgery-related textual concepts. To validate this, we conduct a text-image alignment analysis without training any classifier. We probe whether the frozen embedding space of VLMs naturally clusters synthetic images closer to forgery-related prompts. We constructed a comprehensive text pool categorized into three conceptual groups to probe the model’s internal associations:

- **Forgery-Related Concepts:** Terms explicitly denoting authenticity or fabrication (e.g., ‘fake’, ‘real’, ‘AI generated’, ‘authentic’, ‘manipulated’, ‘synthetic’).
- **Content-Related Concepts:** Neutral descriptions of visual content (e.g., ‘sunset’, ‘landscape’, ‘portrait’, ‘abstract art’, ‘technology’, ‘nature’).
- **Source-Related Concepts:** Specific names of generative models or platforms (e.g., ‘GenImage’, ‘ADM’, ‘BigGAN’, ‘glide’, ‘Midjourney’).

We evaluate the cosine similarity on in-the-wild benchmarks and our newly collected **Midjourney-CC** dataset (3,000 images from [reddit.com/r/midjourney](https://www.reddit.com/r/midjourney), late 2025) to strictly control for data leakage.

Table 5 presents the results of our semantic probing, revealing a striking dichotomy between legacy and modern VLMs. Legacy models like CLIP (2021) and SigLIP (2023) exhibit “forensic blindness,” mapping synthetic images to content terms (e.g., *portrait*). Notably, even the recently released SigLIP 2 (2025) fails to detect forgery concepts (Top-1: *genuine/urban*), likely because it relies on the older WebLI dataset (Chen et al., 2022) curated in 2022, prior to the generative explosion. In sharp contrast, modern VLMs trained on recent web crawls (MetaCLIP 2, PE) consistently align fake images with **“AI generated”**. Crucially, on Midjourney-CC, these models specifically retrieve **“midjourney images”**, providing definitive evidence that their capability stems from exposure to recent, platform-specific metadata which older datasets lack.

Table 5. Comparison of Text-Image Similarities on In-the-Wild Dataset

Method	Chameleon								SocialRF							
	Top-1				Top-2				Top-1				Top-2			
	Matched Text	Similarity Score	Matched Text	Similarity Score	Matched Text	Similarity Score	Matched Text	Similarity Score	Matched Text	Similarity Score	Matched Text	Similarity Score	Matched Text	Similarity Score	Matched Text	Similarity Score
CLIP (2021.2.26) Siglip (2023.3.27) Siglip2 (2025.2.21) Meta CLIP (2023.9.28) Meta CLIP-2 (2025.7.29) PE (2025.4.17)	modern design	0.628	portrait	0.345	forged	0.332	urban	0.253	original	0.222	vintage	0.191	original	0.024	deepfake	0.038
	unaltered	0.318	original	0.212	edited	0.232	original	0.222	vintage	0.191	original	0.024	deepfake	0.038	deepfake	0.031
	genuine	0.385	urban	0.250	portrait	0.202	original	0.191	original	0.024	deepfake	0.038	deepfake	0.031	deepfake	0.031
	AI generated	0.678	deepfake	0.091	AI generated	0.902	original	0.024	deepfake	0.038	deepfake	0.038	deepfake	0.031	deepfake	0.031
	AI generated	0.828	deepfake	0.064	AI generated	0.924	deepfake	0.038	AI generated	0.943	deepfake	0.031	deepfake	0.031	deepfake	0.031
	AI generated	0.861	deepfake	0.021	AI generated	0.943	deepfake	0.031	deepfake	0.031	deepfake	0.031	deepfake	0.031	deepfake	0.031
Method	CommunityAI								Midjourney-CC							
	Top-1				Top-2				Top-1				Top-2			
	Matched Text	Similarity Score	Matched Text	Similarity Score	Matched Text	Similarity Score	Matched Text	Similarity Score	Matched Text	Similarity Score	Matched Text	Similarity Score	Matched Text	Similarity Score	Matched Text	Similarity Score
CLIP (2021.2.26) Siglip (2023.3.27) Siglip2 (2025.2.21) Meta CLIP (2023.9.28) Meta CLIP-2 (2025.7.29) PE (2025.4.17)	portrait	0.346	nature	0.326	urban	0.332	midjourney_images	0.260	midjourney_images	0.260	original	0.246	midjourney_images	0.260	midjourney_images	0.260
	AIGIBench	0.283	real	0.281	fake	0.278	original	0.246	urban	0.212	portrait	0.194	original	0.246	portrait	0.194
	urban	0.209	portrait	0.201	urban	0.212	original	0.194	midjourney_images	0.604	AI generated	0.284	midjourney_images	0.604	AI generated	0.284
	AI generated	0.726	deepfake	0.086	midjourney_images	0.604	AI generated	0.284	AI generated	0.621	AI generated	0.308	midjourney_images	0.604	AI generated	0.308
	AI generated	0.858	deepfake	0.041	midjourney_images	0.621	AI generated	0.308	midjourney_images	0.722	AI generated	0.218	midjourney_images	0.722	AI generated	0.218
	AI generated	0.878	CommunityAI	0.029	midjourney_images	0.722	AI generated	0.218	midjourney_images	0.722	AI generated	0.218	midjourney_images	0.722	AI generated	0.218

Table 6. Counterfactual Analysis. Comparison of DINOv3 trained on Web Data vs. Satellite Data. The satellite model suffers a catastrophic collapse on in-the-wild fakes.

Pre-training Data	GenImage Avg.	Chameleon		
		Real	Fake	Avg.
DINOv3-Web	0.965	0.933	0.895	0.914
DINOv3-Sat	0.706	0.948	0.121	0.535

4.3. Mechanism II: Data-Driven Feature Discrimination in SSL

While VLMs rely on semantic tags, Self-Supervised Learning (SSL) models like DINOv3 lack textual supervision, yet they often outperform VLMs in our benchmarks. We hypothesize that this capability is acquired implicitly through **distribution fitting**: by training on a massive web corpus mixed with generative content, the model learns to encode the distinct **low-level signatures of the generative manifold** into its feature space as separable clusters, independent of semantic labels.

To validate that this capability stems from **data exposure** rather than architectural advantages, we conduct a counterfactual experiment. We employ the identical **DINOv3 ViT-7B** architecture but vary the pre-training data source: **DINOv3-Web (LVD-1689M)**: Pre-trained on a large-scale web corpus containing 1.6 billion diverse internet images, which naturally includes a significant volume of AIGI. **DINOv3-Sat (Sat-493M)**: Pre-trained on 493 million satellite images, a domain strictly devoid of generative content.

Table 6 delivers a decisive finding. While the web-trained baseline excels, DINOv3-Sat completely fails on fake images, despite performing well on real ones. This collapse proves that the model classifies unseen fakes as “real” simply because it is not included in pretrained data. The conclusion is the forensic capability of SSL models is not inherent to the architecture or training strategy, but is entirely contingent on exposure to generative data during pre-training.

Table 7. Robustness to Common Perturbations on Chameleon Dataset. We evaluate the impact of JPEG compression and Gaussian Blur.

Detector	Base (No Aug.)	JPEG Compression (Quality ↓)				Gaussian Blur (σ ↑)			
		95	85	75	65	0.5	1.0	1.5	2.0
MetaCLIP2-Linear	0.644	0.614	0.667	0.614	0.749	0.614	0.744	0.775	0.722
SigLIP2-Linear	0.606	0.583	0.600	0.593	0.605	0.500	0.477	0.482	0.471
DINOv2-Linear	0.608	0.606	0.605	0.606	0.596	0.590	0.564	0.564	0.542
DDA	0.824	0.836	0.823	0.790	0.790	0.844	0.843	0.797	0.758
SigLIP2-Linear	0.858	0.857	0.856	0.860	0.828	0.836	0.776	0.689	0.671
MetaCLIP2-Linear	0.930	0.933	0.940	0.937	0.898	0.922	0.931	0.939	0.932
PE-CLIP-Linear	0.959	0.967	0.964	0.959	0.921	0.938	0.925	0.831	0.778
DINOv3-Linear	0.914	0.918	0.914	0.916	0.891	0.916	0.909	0.897	0.891

5. Robustness and Limitations

5.1. Protocol I: Resilience to Common Perturbations

We conduct our evaluation on the **Chameleon** dataset, which represents the most challenging in-the-wild distribution. We benchmark against **DDA**, the only specialized detector that maintains non-trivial performance on this dataset. We apply varying levels of JPEG compression (Quality $\in \{95, \dots, 65\}$) and Gaussian Blur ($\sigma \in \{0.5, \dots, 2.0\}$) to the test set. As detailed in Table 7, the results reveal a critical trade-off between peak performance and stability among modern VFs. **JPEG compression**, which typically disrupts the specific artifact patterns used by traditional detectors, has a minimal impact on our baselines. This confirms that these models do not rely on fragile high-frequency noise statistics but rather on robust feature representations.

A significant divergence appears under **Gaussian Blur**. **PE-CLIP**, despite establishing the highest baseline accuracy (95.9%), exhibits a sharp performance degradation as blur intensity increases, dropping to **77.8%** at $\sigma = 2.0$. This indicates that PE-CLIP’s superior detection capability is partially driven by fine-grained, high-frequency textual or visual artifacts that are easily erased by smoothing. In sharp contrast, **MetaCLIP2** and **DINOv3** demonstrate remarkable resilience. **MetaCLIP2** actually maintains or slightly improves its accuracy under blur, while **DINOv3** experi-

Table 8. Robustness Evaluation on RRDataset. We report the accuracy on Real and AI classes separately.

Detector	Original (Base)		Redigital (Recapture)		Transfer (Social App)	
	Real	AI	Real	AI	Real	AI
CNNSpot	0.977	0.189	0.986	0.068	0.993	0.065
NPR	0.957	0.749	0.955	0.083	0.998	0.002
SAFE	0.874	0.792	0.928	0.066	0.997	0.009
DDA	0.942	0.895	0.961	0.298	0.933	0.532
SigLIP2-Linear	0.8714	0.931	0.885	0.559	0.490	0.704
MetaCLIP2-Linear	0.784	0.939	0.791	0.719	0.930	0.713
PE-CLIP-Linear	0.925	0.949	0.913	0.548	0.989	0.685
DINOv3-Linear	0.951	0.930	0.964	0.647	0.980	0.712

ences a negligible drop. This indicates that the models capture fundamental structural anomalies inherent to the synthesis process, which are robust to smoothing operations, unlike local pixel-level artifacts. This property makes them ideal candidates for real-world applications involving low-resolution previews or video frame analysis. We also provide additional experiments verifying their efficacy on video detection benchmarks in Appendix B.

5.2. Protocol II: Real-World Transmission and Recapture

To evaluate deployment reliability, we further assess performance under severe image degradation scenarios, including optical recapture from screens and heavy compression introduced by social media transmission protocols. To evaluate this, we utilize the RRDataset (Li et al., 2025a), measuring performance across three settings: **Original** (Digital baseline), **Redigital** (Screen or print recapture), and **Transfer** (Social media transmission).

As detailed in Table 8, specialized detectors suffer a total collapse under transmission and recapture. Methods like SAFE and NPR degrade to near-zero sensitivity on fake images (< 1%). Even the robust DDA drops to 29.8% on recaptured data. In sharp contrast, modern VFMAs maintain robust detection capabilities. **MetaCLIP2-Linear** leads with $\sim 72\%$ accuracy across both scenarios. Consistent with the blur experiments (Sec. 5.1), **PE-CLIP** suffers a notable drop (to 54.8%) on recaptured data, confirming its reliance on fine-grained details prone to erasure by low-pass filtering. Conversely, **DINOv3** and **MetaCLIP2** exhibit superior resilience, suggesting that their learned structural anomalies and semantic concepts persist even through the analog-to-digital bottleneck.

5.3. Protocol III: Robustness to Reconstruction and Editing

While modern VFMAs excel at detecting fully generated images, forensic reliability requires handling subtler manipulations: **(1) VAE Reconstruction**, where a real image is encoded and decoded by a diffusion model’s VAE without semantic modification (simulating deepfake pre-processing);

Table 9. Limitations under Reconstruction and Editing. Detection accuracy on **DDA-COCO** (VAE-based reconstruction) and **BR-Gen** (Diffusion-based local editing).

Method	DDA-COCO			BR-Gen		
	SDXL	SD2	SD3.5L	Brush	Power	SDXL
CNNSpot	0.014	0.017	0.004	0.121	0.091	0.073
DDA	0.949	0.997	0.682	0.648	0.589	0.465
OMAT	0.211	0.304	0.135	0.697	0.715	0.681
Effort	0.511	0.549	0.682	0.801	0.793	0.767
SigLIP2-Linear	0.071	0.079	0.017	0.597	0.623	0.476
MetaCLIP2-Linear	0.057	0.074	0.037	0.544	0.575	0.500
PE-CLIP-Linear	0.066	0.170	0.024	0.564	0.581	0.528
DINOv3-Linear	0.030	0.079	0.004	0.592	0.613	0.450

and **(2) Local Editing**, where only specific regions are inpainted. We evaluate on the **DDA-COCO** (Chen et al., 2025b) (VAE-reconstructed real images) and **BR-Gen** (Cai et al., 2025) (Diffusion-based local editing) datasets.

Table 9 (Left) exposes a critical limitation: modern VFMAs are essentially blind to pure VAE reconstruction artifacts. Detection rates plummet to negligible levels, indicating that these models do not perceive the low-level noise footprint of the VAE decoder as an anomaly. Conversely, **DDA**, which explicitly aligns with VAE reconstruction patterns, maintains robust performance. As shown in Table 9 (Right), VFMAs struggle to generalize to localized manipulations (BR-Gen), with performance hovering around **50%–60%**. We attribute this to the **global pooling mechanism** inherent to our linear probing approach: the dominant feature signal from the unaltered “real” regions likely suppresses the subtle forensic traces within the edited mask. In contrast, methods like **Effort**, designed to amplify anomaly feature, achieve higher accuracy.

6. Conclusion

In this work, we revisited AIGI detection through the lens of the “Bitter Lesson,” demonstrating that simplicity prevails over complex architectural designs. We show that simple linear probes on modern Vision Foundation Models (VFMAs) achieve state-of-the-art performance, decisively outperforming specialized detectors in challenging in-the-wild scenarios. Our analysis traces this capability to pre-training data exposure rather than architectural bias. Modern VFMAs have effectively internalized the “generative manifold” from web-scale data, either through semantic alignment (VLMs) or implicit feature discrimination (SSL). However, we also identify the boundaries of this paradigm: while VFMAs solve the generalization problem for fully synthetic content, they remain blind to fine-grained reconstruction and localized editing. We conclude that the future of AI forensics lies not in hand-crafting artifact extractors, but in harnessing the evolving world knowledge of foundation models. As the line between real and synthetic blurs, leveraging the very models driving this revolution offers the most robust path forward.

References

Baraldi, L., Cocchi, F., Cornia, M., Baraldi, L., Nicolosi, A., and Cucchiara, R. Contrasting deepfakes diffusion via contrastive learning and global-local similarities. In *European Conference on Computer Vision*, pp. 199–216. Springer, 2024.

Bolya, D., Huang, P.-Y., Sun, P., et al. Perception encoder: The best visual embeddings are not at the output of the network. *arXiv preprint arXiv:2504.13181*, 2025.

Cai, L., Wang, H., Ji, J., ZhouMen, Y., Chen, S., Yao, T., and Sun, X. Zooming in on fakes: A novel dataset for localized ai-generated image detection with forgery amplification approach. *arXiv preprint arXiv:2504.11922*, 2025.

Cavia, B., Horwitz, E., Reiss, T., and Hoshen, Y. Real-time deepfake detection in the real-world. *arXiv preprint arXiv:2406.09398*, 2024.

Chen, B., Zeng, J., Yang, J., and Yang, R. Drct: Diffusion reconstruction contrastive training towards universal detection of diffusion generated images. In *Forty-first International Conference on Machine Learning*, 2024a.

Chen, H., Hong, Y., Huang, Z., Xu, Z., Gu, Z., Li, Y., Lan, J., Zhu, H., Zhang, J., Wang, W., et al. Demamba: Ai-generated video detection on million-scale genvideo benchmark. *arXiv preprint arXiv:2405.19707*, 2024b.

Chen, R., Gao, J., Lin, K., Zhang, K., Zhao, Y., Guan, I., Yao, T., and Ding, S. Task-model alignment: A simple path to generalizable ai-generated image detection. *arXiv preprint arXiv:2512.06746*, 2025a.

Chen, R., Xi, J., Yan, Z., et al. Dual data alignment makes ai-generated image detector easier generalizable. *arXiv preprint arXiv:2505.14359*, 2025b.

Chen, X., Wang, X., Changpinyo, S., Piergiovanni, A. J., Padlewski, P., Salz, D., Goodman, S., Grycner, A., Mustafa, B., Beyer, L., et al. Pali: A jointly-scaled multilingual language-image model. *arXiv preprint arXiv:2209.06794*, 2022.

Choi, S., Lee, H., and Lee, M. Training-free detection of ai-generated images via cropping robustness. *arXiv preprint arXiv:2511.14030*, 2025.

Chuang, Y.-S., Li, Y., Wang, D., et al. Metaclip 2: A world-wide scaling recipe. *arXiv preprint arXiv:2507.22062*, 2025.

Coccomin, D. A., Zilos, G. K., Amato, G., Caldelli, R., Falchi, F., Papadopoulos, S., and Gennaro, C. Mintime: Multi-identity size-invariant video deepfake detection. *IEEE Transactions on Information Forensics and Security*, 19:6084–6096, 2024.

Cozzolino, D. and Verdoliva, L. Noiseprint: A cnn-based camera model fingerprint. *IEEE Transactions on Information Forensics and Security*, 15:144–159, 2019.

Doloriel, C. T. and Cheung, N.-M. Frequency masking for universal deepfake detection. In *ICASSP 2024-2024 IEEE International Conference on Acoustics, Speech and Signal Processing (ICASSP)*, pp. 13466–13470. IEEE, 2024.

Frank, J., Eisenhofer, T., Schönherr, L., Fischer, A., Kolossa, D., and Holz, T. Leveraging frequency analysis for deep fake image recognition. In *International conference on machine learning*, pp. 3247–3258. PMLR, 2020.

Gu, Z., Chen, Y., Yao, T., Ding, S., Li, J., Huang, F., and Ma, L. Spatiotemporal inconsistency learning for deepfake video detection. In *Proceedings of the 29th ACM international conference on multimedia*, pp. 3473–3481, 2021.

Internò, C., Geirhos, R., Olhofer, M., Liu, S., Hammer, B., and Klindt, D. Ai-generated video detection via perceptual straightening. *arXiv preprint arXiv:2507.00583*, 2025.

Ju, Y., Jia, S., Ke, L., Xue, H., Nagano, K., and Lyu, S. Fusing global and local features for generalized ai-synthesized image detection. In *2022 IEEE International Conference on Image Processing (ICIP)*, pp. 3465–3469. IEEE, 2022.

Koutlis, C. and Papadopoulos, S. Leveraging representations from intermediate encoder-blocks for synthetic image detection. In *European Conference on Computer Vision*, pp. 394–411. Springer, 2024.

Li, C., Wang, X., Li, M., Miao, B., Sun, P., Zhang, Y., Ji, X., and Zhu, Y. Bridging the gap between ideal and real-world evaluation: Benchmarking ai-generated image detection in challenging scenarios. In *Proceedings of the IEEE/CVF International Conference on Computer Vision*, pp. 20379–20389, 2025a.

Li, O., Cai, J., Hao, Y., Jiang, X., Hu, Y., and Feng, F. Improving synthetic image detection towards generalization: An image transformation perspective. In *Proceedings of the 31st ACM SIGKDD Conference on Knowledge Discovery and Data Mining V. 1*, pp. 2405–2414, 2025b.

Li, Y., Zheng, W., Zhang, Y., Sun, R., Zheng, Y., Chen, L., Zhou, J., and Lu, J. Skyra: Ai-generated video detection via grounded artifact reasoning. *arXiv preprint arXiv:2512.15693*, 2025c.

Li, Z., Yan, J., He, Z., Zeng, K., Jiang, W., Xiong, L., and Fu, Z. Is artificial intelligence generated image detection a solved problem? *arXiv preprint arXiv:2505.12335*, 2025d.

Liu, H., Tan, Z., Tan, C., Wei, Y., Wang, J., and Zhao, Y. Forgery-aware adaptive transformer for generalizable synthetic image detection. In *Proceedings of the IEEE/CVF Conference on Computer Vision and Pattern Recognition*, pp. 10770–10780, 2024.

Liu, Z., Qi, X., and Torr, P. H. Global texture enhancement for fake face detection in the wild. In *Proceedings of the IEEE/CVF conference on computer vision and pattern recognition*, pp. 8060–8069, 2020.

McCloskey, S. and Albright, M. Detecting gan-generated imagery using saturation cues. In *2019 IEEE international conference on image processing (ICIP)*, pp. 4584–4588. IEEE, 2019.

Ni, B., Peng, H., Chen, M., Zhang, S., Meng, G., Fu, J., Xiang, S., and Ling, H. Expanding language-image pre-trained models for general video recognition. In *European conference on computer vision*, pp. 1–18. Springer, 2022.

Odena, A., Dumoulin, V., and Olah, C. Deconvolution and checkerboard artifacts. *Distill*, 2016. doi: 10.23915/distill.00003. URL <http://distill.pub/2016/deconv-checkerboard>.

Ojha, U., Li, Y., and Lee, Y. J. Towards universal fake image detectors that generalize across generative models. In *Proceedings of the IEEE/CVF Conference on Computer Vision and Pattern Recognition*, pp. 24480–24489, 2023.

Oquab, M., Dariseti, T., Moutakanni, T., Vo, H., Szafraniec, M., Khalidov, V., Fernandez, P., Haziza, D., Massa, F., El-Nouby, A., et al. Dinov2: Learning robust visual features without supervision. *arXiv preprint arXiv:2304.07193*, 2023.

Radford, A., Kim, J. W., Hallacy, C., Ramesh, A., Goh, G., Agarwal, S., Sastry, G., Askell, A., Mishkin, P., Clark, J., et al. Learning transferable visual models from natural language supervision. In *International conference on machine learning*, pp. 8748–8763. PMLR, 2021.

Rombach, R., Blattmann, A., Lorenz, D., Esser, P., and Ommer, B. High-resolution image synthesis with latent diffusion models. *arxiv* 2022. *arXiv preprint arXiv:2112.10752*, 2021.

Sha, Z., Li, Z., Yu, N., and Zhang, Y. De-fake: Detection and attribution of fake images generated by text-to-image generation models. In *Proceedings of the 2023 ACM SIGSAC conference on computer and communications security*, pp. 3418–3432, 2023.

Siméoni, O., Vo, H. V., Seitzer, M., Baldassarre, F., Oquab, M., Jose, C., Khalidov, V., Szafraniec, M., Yi, S., Ramamonjisoa, M., et al. Dinov3. *arXiv preprint arXiv:2508.10104*, 2025.

Sutton, R. The bitter lesson. *Incomplete Ideas (blog)*, 13(1): 38, 2019.

Tan, C., Zhao, Y., Wei, S., Gu, G., Liu, P., and Wei, Y. Frequency-aware deepfake detection: Improving generalizability through frequency space domain learning. In *Proceedings of the AAAI Conference on Artificial Intelligence*, volume 38, pp. 5052–5060, 2024a.

Tan, C., Zhao, Y., Wei, S., Gu, G., Liu, P., and Wei, Y. Rethinking the up-sampling operations in cnn-based generative network for generalizable deepfake detection. In *Proceedings of the IEEE/CVF Conference on Computer Vision and Pattern Recognition*, pp. 28130–28139, 2024b.

Tan, C., Tao, R., Liu, H., et al. C2p-clip: Injecting category common prompt in clip to enhance generalization in deepfake detection. In *Proceedings of the AAAI Conference on Artificial Intelligence*, volume 39, pp. 7184–7192, 2025.

Team, G., Anil, R., Borgeaud, S., Alayrac, J.-B., Yu, J., Soricut, R., Schalkwyk, J., Dai, A. M., Hauth, A., Millican, K., et al. Gemini: a family of highly capable multimodal models. *arXiv preprint arXiv:2312.11805*, 2023.

Tschannen, M., Gritsenko, A., Wang, X., et al. Siglip 2: Multilingual vision-language encoders with improved semantic understanding, localization, and dense features. *arXiv preprint arXiv:2502.14786*, 2025.

Wang, S.-Y., Wang, O., Zhang, R., Owens, A., and Efros, A. A. Cnn-generated images are surprisingly easy to spot... for now. In *Proceedings of the IEEE/CVF conference on computer vision and pattern recognition*, pp. 8695–8704, 2020.

Wang, Z., Bao, J., Zhou, W., et al. Dire for diffusion-generated image detection. In *Proceedings of the IEEE/CVF International Conference on Computer Vision*, pp. 22445–22455, 2023.

Xu, H., Xie, S., Tan, X. E., Huang, P.-Y., Howes, R., Sharma, V., Li, S.-W., Ghosh, G., Zettlemoyer, L., and Feichtenhofer, C. Demystifying clip data. *arXiv preprint arXiv:2309.16671*, 2023a.

Xu, Y., Liang, J., Jia, G., Yang, Z., Zhang, Y., and He, R. Tall: Thumbnail layout for deepfake video detection. In *Proceedings of the IEEE/CVF international conference on computer vision*, pp. 22658–22668, 2023b.

Yan, S., Li, O., Cai, J., Hao, Y., Jiang, X., Hu, Y., and Xie, W. A sanity check for ai-generated image detection. *arXiv preprint arXiv:2406.19435*, 2024a.

Yan, Z., Wang, J., Jin, P., Zhang, K.-Y., Liu, C., Chen, S., Yao, T., Ding, S., Wu, B., and Yuan, L. Orthogonal subspace decomposition for generalizable ai-generated image detection. *arXiv preprint arXiv:2411.15633*, 2024b.

Yang, Y., Qian, Z., Zhu, Y., Russakovsky, O., and Wu, Y. D³ 3: Scaling up deepfake detection by learning from discrepancy. In *Proceedings of the Computer Vision and Pattern Recognition Conference*, pp. 23850–23859, 2025.

Zhai, X., Mustafa, B., Kolesnikov, A., and Beyer, L. Sigmoid loss for language image pre-training. In *Proceedings of the IEEE/CVF international conference on computer vision*, pp. 11975–11986, 2023.

Zhang, S., Lian, Z., Yang, J., Li, D., Pang, G., Liu, F., Han, B., Li, S., and Tan, M. Physics-driven spatiotemporal modeling for ai-generated video detection. *arXiv preprint arXiv:2510.08073*, 2025.

Zheng, C., Lin, C., Zhao, Z., Wang, H., Guo, X., Liu, S., and Shen, C. Breaking semantic artifacts for generalized ai-generated image detection. *Advances in Neural Information Processing Systems*, 37:59570–59596, 2024.

Zheng, Y., Bao, J., Chen, D., Zeng, M., and Wen, F. Exploring temporal coherence for more general video face forgery detection. *2021 IEEE/CVF International Conference on Computer Vision (ICCV)*, pp. 15024–15034, 2021.

Zhou, Y., He, X., Lin, K., Fan, B., Ding, F., and Li, B. Breaking latent prior bias in detectors for generalizable aigc image detection. *arXiv preprint arXiv:2506.00874*, 2025a.

Zhou, Z., Luo, Y., Wu, Y., Sun, K., Ji, J., Yan, K., Ding, S., Sun, X., Wu, Y., and Ji, R. Aigi-holmes: Towards explainable and generalizable ai-generated image detection via multimodal large language models. *arXiv preprint arXiv:2507.02664*, 2025b.

Zhu, M., Chen, H., Yan, Q., et al. Genimage: A million-scale benchmark for detecting ai-generated image. *Advances in Neural Information Processing Systems*, 36: 77771–77782, 2023.

A. Survey of Backbones in Recent AIGI Detection Methods

To contextualize our work within the current literature, we provide a comprehensive survey of the backbones utilized by state-of-the-art AIGI detection methods published between 2023 and 2025. As shown in Table 10, the vast majority of recent methods rely on legacy architectures, primarily the original CLIP ViT-L/14 (released in early 2021) or standard ResNet-50. Only a few recent works (e.g., DDA) have begun to explore newer self-supervised models like DINOv2. This highlights a significant lag in the forensics community in adopting the latest generation of foundation models, further motivating our investigation into modern VFM like MetaCLIP 2, SigLIP 2, and DINOv3.

Table 10. Backbone Architectures in Recent AIGI Detection Methods (2023–2025). The table surveys representative methods from top-tier venues. Most existing works are built upon legacy backbones such as OpenAI CLIP (2021) or ResNet-50, lacking exposure to the modern generative web distribution.

Method	Year	Venue	Key Backbone(s)	Note
UnivFD (Ojha et al., 2023)	2023	CVPR	CLIP-ViT (ViT-L/14)	Pioneered CLIP for forensics
DE-FAKE (Sha et al., 2023)	2023	CCS	CLIP-ViT (ViT-L/14), ResNet-18	Multi-modal features
FatFormer (Liu et al., 2024)	2024	CVPR	CLIP-ViT (ViT-L/14)	Adaptive Transformer
NPR (Tan et al., 2024b)	2024	CVPR	ResNet-18 (Lightweight)	Neighboring Pixel Reconstruction
RINE (Koutlis & Papadopoulos, 2024)	2024	ECCV	CLIP ViT-L/14, ViT-B/32	Intermediate representations
CoDE (Baraldi et al., 2024)	2024	ECCV	ViT-Tiny	Contrastive learning
DRCT (Chen et al., 2024a)	2024	ICML	ConvNeXt-Base, CLIP-ViT (ViT-L/14)	Reconstruction discrepancy
Patch Shuffle (Zheng et al., 2024)	2024	NeurIPS	ResNet-50	Breaking semantic artifacts
C2P-CLIP (Tan et al., 2025)	2025	AAAI	CLIP-ViT (ViT-L/14)	Prompt tuning
SAFE (Li et al., 2025b)	2025	KDD	ResNet-50 (Lightweight)	Image transformation
AIDE (Yan et al., 2024a)	2025	ICLR	ResNet-50, OpenCLIP (ConvNeXt)	Frequency analysis
Effort (Yan et al., 2024b)	2025	ICML	CLIP-ViT (ViT-L/14)	Orthogonal decomposition
D3 (Yang et al., 2025)	2025	CVPR	CLIP-ViT (ViT-L/14)	Discrepancy learning
DDA (Chen et al., 2025b)	2025	NeurIPS	DINOv2	Dual Data Alignment
OMAT (Zhou et al., 2025a)	2025	NeurIPS	CLIP-ViT (ViT-L/14)	Latent prior bias
WaRPAD (Choi et al., 2025)	2025	NeurIPS	DINOv2	Cropping Robustness

B. Generalization to Video Forgery Detection.

To further evaluate the versatility of the advanced VFM paradigm, we extend our analysis to the temporal domain. We hypothesize that the robust feature representations learned by the latest Vision Foundation Models (VFM) are not merely restricted to static artifacts but possess inherent cross-task generalization capabilities for video detection.

Methodology and Experimental Setup. For video inference, we employ a straightforward temporal aggregation strategy. Given an input video sequence, we extract a continuous segment of S frames (where $S_{max} = 8$). Each frame is processed independently through the frozen VFM backbone to generate frame-level logits. The final prediction for the entire video sequence is derived by calculating the mean of the aggregated logits across all S frames. This approach allows us to leverage the VFM’s ‘firepower’ without the need for specialized temporal architectures or costly fine-tuning on video-specific datasets.

We conducted benchmarks on two prominent datasets: VidproM and GenVideo. Performance is measured using the Recall metric for synthetic subsets (e.g., LaVie, Hotshot, Sora) to assess detection sensitivity.

Observations on Scaling and Quality. The results, summarized in Tab ??, reveal a clear correlation between the ‘scale-up’ of VFM parameters/data and their zero-shot detection efficacy. For lower-quality video generation models like LaVie and Hotshot, there is a dramatic performance leap across VFM generations. For instance, while a standard CLIP backbone achieves a mediocre Recall of 62.93% on LaVie, the SigLIP model pushes this to 79.21%. Remarkably, latest-generation VFM like DINOv3 and MetaCLIP-2 decisively dominate these benchmarks with Recall rates exceeding 90%.

Interestingly, this performance gain remains evident, albeit less pronounced, when faced with high-fidelity outputs from advanced generators like Sora. Even as the visual quality of forgeries improves, the detection capability of the latest VFM continues to scale linearly with the model’s pre-training breadth. Perhaps most significantly, despite the absence of video-specific training or official temporal supervision, these general-purpose ‘guns’ consistently outperform bespoke AI video detectors specifically designed for these tasks.

Table 11. Cross-task Generalization to Video Forgery Detection (VidProm).

Method	Accuracy ↑ (%)				
	Pika	VC2	T2VZ	MS	Avg
CNNSpot (Wang et al., 2020)	0.5117	0.5018	0.4997	0.5031	0.5041
FrDect (Doloriel & Cheung, 2024)	0.5007	0.5403	0.6988	0.6994	0.6098
Fusing (Ju et al., 2022)	0.5060	0.5007	0.4981	0.5128	0.5044
Gram-Net (Liu et al., 2020)	0.8419	0.6742	0.5248	0.5046	0.6364
GIA (Frank et al., 2020)	0.5373	0.5175	0.4105	0.6022	0.5169
UnivFD (Ojha et al., 2023)	0.4941	0.4865	0.4958	0.5743	0.5127
ReStraV (Internò et al., 2025)	0.9090	0.9950	0.9905	0.9837	0.9706
CLIP	0.9637	0.7764	0.8535	0.1093	0.6757
SigLIP	0.3867	0.9057	0.9987	0.8278	0.7797
SigLIP2	0.7540	0.9896	0.9967	0.9928	0.9333
PE	0.9857	0.9992	0.9926	0.8115	0.9473
MetaCLIP-v2	0.9784	0.9982	0.9971	0.8762	0.9625
DinoV3	0.9985	0.9988	0.9764	0.9768	0.9876

Table 12. Cross-task Generalization to Video Forgery Detection (GenVideo).

Model	Testing Subset										Avg.
	Sora	Morph Studio	Gen2	HotShot	Lavie	Show-1	Moon Valley	Crafter	Model Scope	Wild Scrape	
NPR (Tan et al., 2024b)	0.5536	0.7757	0.7188	0.4860	0.0721	0.0429	0.8626	0.6029	0.7143	0.3153	0.5144
STIL (Gu et al., 2021)	0.7500	0.7943	0.9449	0.5786	0.5314	0.6414	0.9712	0.8529	0.6943	0.6242	0.7383
MINTIME-CLIP-B (Cocomomi et al., 2024)	0.1607	0.2686	0.1471	0.0557	0.3757	0.0900	0.2188	0.4071	0.0114	0.4309	0.2166
FTCN-CLIP-B (Zheng et al., 2021)	0.9107	0.9300	0.9232	0.1771	0.1750	0.0643	0.9968	0.8479	0.7457	0.5173	0.6287
TALL (Xu et al., 2023b)	0.6071	0.7043	0.9449	0.5914	0.5757	0.6400	0.9633	0.8871	0.6057	0.6210	0.7141
XCLIP-B-FT (Ni et al., 2022)	0.6786	0.9129	0.9623	0.1200	0.2236	0.0914	0.9984	0.8343	0.7557	0.5184	0.6096
DeMamba-XCLIP-FT (Chen et al., 2024b)	0.9286	0.9729	0.9848	0.3829	0.5350	0.4143	0.9984	0.9407	0.7729	0.6415	0.7572
NSG-VD (Zhang et al., 2025)	0.7857	0.9833	0.8000	0.9250	0.9417	0.8750	1.0000	0.9833	0.6833	0.8250	0.8802
Skyra-RL-GenVideo(7B) (Li et al., 2025c)	0.9564	0.9586	0.9623	0.8271	0.9429	0.7200	0.9792	0.9807	0.6629	0.7863	0.8766
CLIP	0.5857	0.9200	0.8942	0.3471	0.6293	0.3100	0.9840	0.9886	0.8557	0.6090	0.7124
SigLIP	0.5000	0.5771	0.3949	0.8429	0.7921	0.7729	0.3626	0.6767	0.2571	0.6982	0.5875
SigLIP2	0.3214	0.9314	0.9036	0.6914	0.7971	0.8600	0.9968	0.9850	0.8129	0.7258	0.8025
PE	0.4286	0.9657	0.9884	0.8114	0.8936	0.7900	1.0000	0.9964	0.9543	0.8216	0.8650
MetaCLIP-v2	0.6871	0.9914	0.9884	0.8300	0.9036	0.8714	1.0000	1.0000	0.9543	0.7148	0.8941
DinoV3	0.6250	0.9957	0.9928	0.9214	0.9571	0.9500	1.0000	0.9971	0.9743	0.7302	0.9144

C. Model Architectures and Training Details

In this section, we provide detailed specifications for the Vision Foundation Model (VFM) backbones employed in our study. As summarized in Table 13, we selected a diverse set of state-of-the-art architectures to benchmark the “Simplicity Prevails” hypothesis.

Backbone Selection. Our evaluation suite encompasses two distinct pre-training paradigms:

- **Vision-Language Models (VLMs):** Including the **MetaCLIP** and **SigLIP** families, alongside the video-enhanced **Perception Encoder (PE)**. These models are pre-trained on billion-scale image-text pairs (e.g., WebLI, Common Crawl), equipping them with the semantic understanding required for the zero-shot concept alignment observed in our experiments.
- **Self-Supervised Models (SSL):** Specifically the **DINO** family. Notably, we utilize the massive **DINOv3** (ViT-7B architecture) trained on the LVD-1689M dataset. This uncurated visual exposure allows the model to learn structural forensic features without textual supervision.

Implementation. Consistent with our protocol, all backbones are frozen during training. We attach a simple linear layer to the feature dimension specified in the table. Input images are resized to the native resolution of each model (e.g., 384 × 384 for SigLIP models) to ensure optimal feature extraction.

Table 13. Backbone Models and Training Specifications. We detail the specific architectures, input resolutions, and pre-training data sources for all VFM baselines evaluated in this work.

Detector	Backbone Family	Specific Model	Feature Dim	Input Size	Training Data
<i>Vision Transformers (CLIP-based)</i>					
MetaCLIP-Linear	CLIP	MetaCLIP-H/14-2.5B	1280	224×224	MetaCLIP 400M
MetaCLIP2-Linear	CLIP	MetaCLIP-2 Worldwide Giant	1664	224×224	Common Crawl (Curated)
SigLIP-Linear	CLIP	SigLIP-Large/16	1024	384×384	WebLI (Chen et al., 2022)
SigLIP2-Linear	CLIP	SigLIP-2 Giant/16	1536	384×384	WebLI (Chen et al., 2022)
PE-CLIP-Linear	CLIP	PE-Core-L/14	1024	336×336	MetaCLIP Images + 22M Videos
<i>Vision Transformers (Self-supervised)</i>					
DINOv2-Linear	DINO	DINOv2-giant	1536	224×224	LVD-142M
DINOv3-Linear	DINO	DINOv3-ViT-7B/16	1664	224×224	LVD-1689M

Notes: (1) CLIP-based models are trained on image-text pairs; DINO models use self-distillation. (2) Data sources: WebLI (Chen et al., 2022); LVD datasets (Oquab et al., 2023). (3) All detectors use frozen backbones with linear heads trained on the **GenImage** dataset.